Available online at www.sciencedirect.com

ScienceDirect

Ceramics International 40 (2014) 4579–4590

CERAMICS INTERNATIONAL

www.elsevier.com/locate/ceramint

Evaluation of hot corrosion behavior of CSZ, CSZ/micro Al_2O_3 and CSZ/nano Al_2O_3 plasma sprayed thermal barrier coatings

M. Nejati, M.R. Rahimipour, I. Mobasherpour*

Ceramics Department, Materials and Energy Research Center, P.O. Box 31787-316, Karaj, Iran

Received 7 July 2013; received in revised form 31 August 2013; accepted 31 August 2013
Available online 20 September 2013

Abstract

Hot corrosion is one of the main destructive factors in thermal barrier coatings (TBCs) which come as a result of molten salt effect on the coating–gas interface. Hot corrosion behavior of three types of plasma sprayed TBCs was evaluated: usual CSZ, layer composite of CSZ/Micro Al_2O_3 and layer composite of CSZ/Nano Al_2O_3 in which Al_2O_3 was as a topcoat on CSZ layer. Hot corrosion studies of plasma sprayed thermal barrier coatings (TBCs) were conducted in 45 wt% Na_2SO_4+55 wt% V_2O_5 molten salt at 1050 °C for 40 h. The graded microstructure of the coatings was examined using scanning electron microscope (SEM) and X-ray diffractometer (XRD) before and after hot corrosion test. The results showed that no damage and hot corrosion products was found on the surface of CSZ/Nano Al_2O_3 coating and monoclinic ZrO_2 fraction was lower in CSZ/Micro Al_2O_3 coating in comparison with usual CSZ. reaction of molten salts with stabilizers of zirconia (Y_2O_3 and CeO_2) that accompanied by formation of monoclinic zirconia, irregular shape crystals of YVO_4, $CeVO_4$ and semi-cubic crystals of CeO_2 as hot corrosion products, caused the degradation of CSZ coating in usual CSZ and CSZ/Micro Al_2O_3 coating.

Keywords: Thermal barrier coating; Hot corrosion; Plasma spray; CSZ/Al_2O_3 composite

1. Introduction

Ceramic thermal barrier coatings (TBCs) are frequently used in gas turbine engines to provide thermal insulation to the hot-section metallic components (vanes, blades, shrouds, etc.) and also to protect them from oxidation, hot corrosion and erosion, extending the components thermo-mechanical life [1,2]. A typical TBC system includes MCrAlY (M=Ni and/or Co) metallic bondcoat as oxidation resistant layer and partially stabilized zirconia topcoat as thermal insulation layer. The metallic bondcoat is deposited between the metallic substrate and ceramic topcoat to protect the underlying metal (Ni-based superalloys) from oxidation and high temperature corrosion and to enhance the adherence between the dissimilar substrate and topcoat [3–6].

Nowadays, TBCs are usually produced by either atmospheric plasma spraying (APS) or electron beam physical vapor deposition (EB-PVD) [7–9]. However, due to the comparatively cost-effective deposition conditions and high deposition efficiency, plasma spraying technology has enjoyed widespread acceptance up to now [10,11].

Various attempts have been made to improve the coating properties. One of the most important approaches is to substitute Y_2O_3 with more acidic stabilizer elements for partially stabilization of zirconia such as CeO_2, Sc_2O_3, $YTaO_4$ and In_2O_3 [12–14]. Among these TBC systems, ceria stabilized zirconia (CSZ) TBCs have been intensively investigated. Some investigators have reported that the CSZ coatings in addition to high temperature stability, good corrosion resistance and high fracture toughness, also have lower thermal conductivity and higher thermal expansion coefficient than YSZ coatings [15–18].

Partially stabilized zirconia coatings exhibit a poor hot corrosion resistance to the molten salt contaminants such as Na_2SO_4 and V_2O_5 etc, arising from the use of low-quality fuels [19–22]. Stabilizers will leach out by the reaction with V_2O_5 or $NaVO_3$ to form corrosion products, resulting in the transformation of tetragonal (t) or cubic (c) zirconia to monoclinic (m) zirconia accompanied by a destructive volume expansion (3–5%), which finally leads to spallation of partially stabilized

*Corresponding author. Tel.: +98 2616204131; fax: +98 26 36201888.
E-mail addresses: I_Mobasherpour@merc.ac.ir, Iman.Mobasherpour@gmail.com (I. Mobasherpour).

0272-8842/$ - see front matter © 2013 Elsevier Ltd and Techna Group S.r.l. All rights reserved.
http://dx.doi.org/10.1016/j.ceramint.2013.08.135

zirconia topcoat [23]. In recent years, different attempts have been made to improve the hot corrosion resistance of thermal barrier coatings that one of the most promising approach is reduce the infiltration of corrosive salts into TBCs structure via deposition of a dense overlay coating over the partially stabilized zirconia coating (that is called double ceramic topcoat system) [24–29].

As regards that Al_2O_3 has a high melting point and is more stable in chemical environment and considered as a oxygen barrier structure in comparison with ZrO_2 and also is not soluble within ZrO_2 [24,29,30], it seems that deposition of a dense Al_2O_3 layer over the partially stabilized zirconia coating in atmospheric plasma sprayed TBCs can significantly reduce infiltration of molten salts into the TBC structure and results in increasing of resistance to hot corrosion [25,28]. Alumina undergoes several crystallographic modifications during thermal spraying related to the cooling rate of the deposit. Metastable transformations decrease the coating mechanical properties, such as the fracture toughness, and reduce their tribological applications [31] and these unstable phases will transform into stable α-Al_2O_3 during thermal cycling, accompanied by a significant volume change ($\gamma \rightarrow \alpha$, ~15%) which results in micro crack formation in the coating [32].

In recent years, nanostructured coatings deposited by atmospheric plasma spraying have attracted some research interest because of some superior properties than that of conventional coatings [33–36], however, few publications on plasma-sprayed nanostructured TBCs have been released. The exceptional properties of nanostructured materials have been documented for both bulk materials and coatings. Proper deposition of nanostructured plasma sprayed ceramic coatings by taking advantage of properties associated with nanostructures, can advance the performance and durability of conventional plasma sprayed coatings that already have a wide variety of applications [37]. Plasma sprayed nanostructured coatings show improvement of resistance to wear, erosion, corrosion and mechanical properties are also improved as compare their conventional counterparts [38].

Therefore, the main purpose of this research is formation of two types of alumina coatings from nano and micron size powders to improve the hot corrosion resistance of usual TBC by a dense alumina overlay as third layer in TBC system and comparison of hot corrosion behavior of nanostructured and conventional alumina overlay coatings. To this end, three types of plasma sprayed TBC were produced: usual CSZ, layer composite of CSZ/Micro Al_2O_3 and layer composite of CSZ/Nano Al_2O_3. Then these three types of coatings have been investigated by observation of microstructure and chemical analysis before and after hot corrosion test.

2. Material and methods

2.1. As-received materials

Inconel 738LC superalloy which grit blasted with alumina particles was used as the substrate with the dimension of 25 mm × 17 mm × 10 mm. Four types of commercial powders were used: Amdry 962 (Ni–22Cr–10Al–1Y, −106+52 μm) as bondcoat, Metco 205NS-G (ZrO_2–$24CeO_2$–$2.5Y_2O_3$, −125+11 μm), Metco 105NS (high purity alpha Al_2O_3, −45+15 μm) and US3008 (high purity nano alpha Al_2O_3, 80 nm) as TBC or ceramic layer. Three types of coatings were produced by air plasma spray (APS) method, which included: usual CSZ, layer composite of CSZ/Micro Al_2O_3 in which micro Al_2O_3 layer was as a topcoat on the surface of CSZ and layer composite of CSZ/Nano Al_2O_3 in which nano Al_2O_3 layer was as a topcoat on the surface of CSZ. Table 1 indicates the characteristics of the coatings.

2.2. Granulation of nano Al_2O_3 powders

Micro alumina powder could be fed directly in the air plasma spray system. However, it is impossible for nano Al_2O_3 powder due to its lower inertia force; the nano powder cannot penetrate the hot gas downstream. Even if it can penetrate into the plasma plume, particles will be easily vaporized because of the low mass. This is the reason why the nano powder particles need to be granulated. The spray drying technique is used to granulate the nano powder. A specific amount of hydro soluble polyvinyl alcohol (PVA) (Junsel Chemical Co. Ltd., Japan) as binder was first added to distilled water and stirred for 20 min at 40 °C until PVA was completely soluble. Then the nano Al_2O_3 powder was gradually added and the suspension was stirred again for an additional 15 min and dispersed slurry. After granulation, granules dried for 12 h at 200 °C and could be fed in the air plasma spray system.

Table 1
Types of TBCs and thickness of layers (μm).

Type of TBC	NiCrAlY	CSZ[a]	Micro Al_2O_3	Nano Al_2O_3	Abbreviation
Usual	150	350	–	–	CSZ
Layer composite	150	250	100	–	CSZ/Micro Al_2O_3
Layer composite	150	250	–	100	CSZ/Nano Al_2O_3

[a]CSZ: ceria stabilized zirconia.

Table 2
Parameters of air plasma spraying.

Parameter	NiCrAlY	CSZ	Nano Al_2O_3	Micro Al_2O_3
Current (A)	400	550	550	550
Voltage (V)	80	70	70	70
Primary gas, Ar (l/min)	55	38	38	38
Secondary gas, H_2 (i/min)	17	17	17	17
Powder feed rate (g/min)	40	30	30	30
Spray distance (cm)	15	8	8	8

2.3. Air plasma spraying

Plasma spraying was carried out with a Plasma Technique AG; Metco 3 MB gun in air. Argon gas was the primary plasma gas and hydrogen gas was added as the secondary gas. The powders were sprayed based on the standard parameters suggested by the Sulzer-Metco. Spraying parameters are shown in Table 2. In order to increase the surface roughness and coating adhesion, the substrates were grit blasted with alumina particles. They were also degreased and cleaned with acetone and preheated with plasma gun prior to spraying. The sprayed coating, which was formed directly on the substrate, was cooled by air blowing onto the surface.

2.4. Microstructure analysis

The microstructure and chemical composition of the coatings before and after hot corrosion test were analyzed by scanning electron microscopy (SEM: VEGA//TESCAN-XMU, Russia) equipped with energy dispersive spectrometer (EDS). For such analysis, selected samples were sectioned with a low-velocity diamond saw and cross-section was cold-mounted in vacuum in epoxy resin, then polished. The samples were dried and gold coated using a Sputter Coater System. The phase analysis of coatings was performed by using an X-ray diffractometer (XRD: unisantis MD300, Germany), operating with Cu Kα radiation at 45 kV and 1 mA. The analyzed range of the diffraction angle (2θ) was between 20° and 80°, with a step width of 0.02°.

Table 3
Physical specifications of corrosive salts.

Type of salt	Manufacturer	Melting point (°C)	Density (g/cm^3)
Na_2SO_4	Merck (Germany)	888	2.70
V_2O_5	Merck (Germany)	690	3.36

2.5. Hot corrosion test

In order to evaluate corrosion behavior of coatings, a mixture of 55 wt% V_2O_5 and 45 wt% Na_2SO_4 powders was selected as a corrosive salt. Some specifications of each salt are presented in Table 3. The corrosive salt was strewed over the surface of coatings in a 30 mg/cm^2 concentration leaving approximately 3 mm from the uncoated edge to avoid edge effect. The specimens were set in an electric furnace with air atmosphere at 1050 °C for 40 h and then cooled down inside the furnace. The specimens were visual inspected periodically every 4 h.

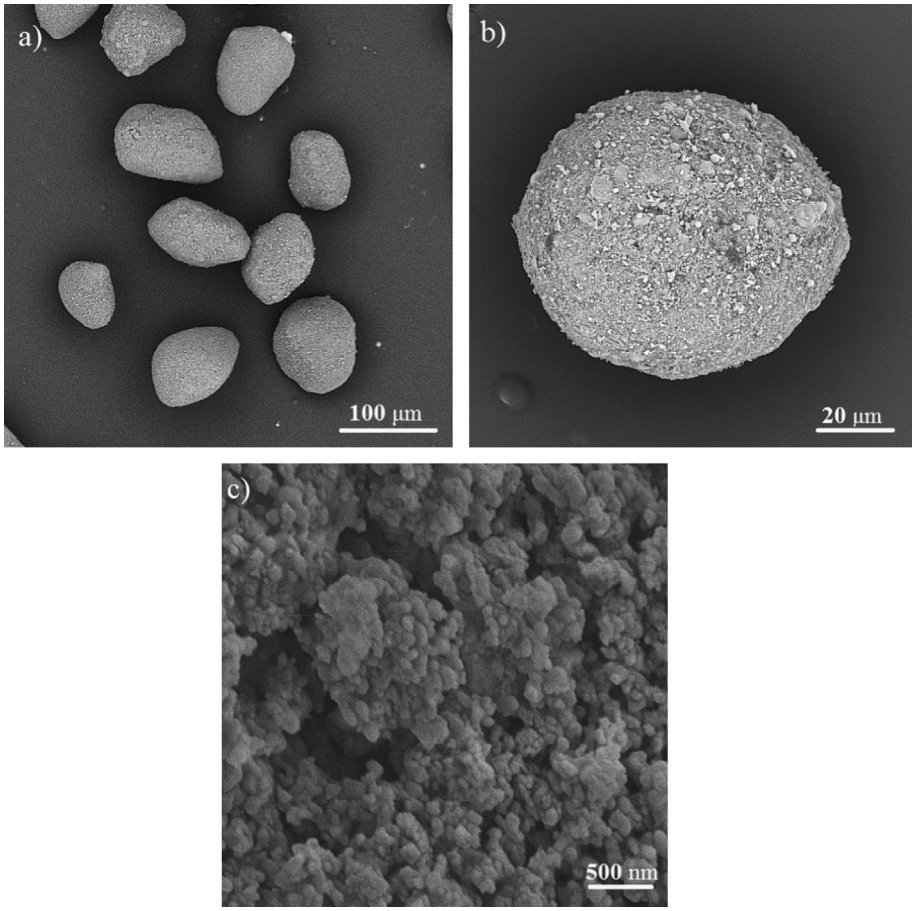

Fig. 1. (a) Morphology of granulated nano Al_2O_3 powders after granulation, and (b), (c) higher magnification of surface of a granule.

3. Results and discussion

3.1. Microstructure of the granulated nano Al_2O_3 powders

Fig. 1(a) shows the morphology of nano Al_2O_3 powders after granulation process. As can be observed in Fig. 1(b) and(c), a granulated particle which can be considered as a plasma spray able powder in APS method, is composed of a large number of nano Al_2O_3 particles. The diameter of nano powder after granulation has become 65 to 80 μm. Comparing with original powder, it would possess the better flow ability since the weight of single particle is increased.

3.2. Characterization of as-sprayed coatings

Fig. 2 shows the polished cross-section of the three types of TBCs. In Fig. 2(a), usual TBC is observed which includes bondcoat and CSZ layers. In Fig. 2(b) and (c), the topcoat is Al_2O_3 layer and CSZ coating is between alumina layer and bondcoat. Fig. 2(d) indicates that the nano Al_2O_3 overlay in CSZ/Nano Al_2O_3 coating, after plasma spraying shows a bimodal microstructure that containing the fully molten and semi-molten nanostructured granules. The image analysis results indicated that the porosity of CSZ, micro Al_2O_3 and nano Al_2O_3 coatings are 10.6%, 3.2% and 4.4% respectively. All of the coatings showed the lamellar structure which is a characteristic of plasma sprayed coatings [24]. Fig. 3 shows the top surface of the three types of TBCs. As shown in Fig. 3, the top surfaces of the coatings are very rough because it includes of splats that deposited on surface with different flattening parameters. Microcracks, porosity and occasional unmelted particles are also visible on the top surface of coatings. These defects are common characteristics of plasma sprayed TBCs that play an important role in hot corrosion behavior of TBC system as effective penetration paths of molten salts [15]. Fig. 3(d) shows the high magnification view of top surface of nano Al_2O_3 layer that exhibit a semi-molten nanostructured feedstock particle embedded in the coating microstructure. The XRD analysis was performed on the top surface of the coatings before hot corrosion. Fig. 4 illustrates the XRD patterns of as-sprayed CSZ, CSZ/Micro Al_2O_3 and CSZ/Nano Al_2O_3 TBCs. According to these patterns, CSZ consisted of no transformable tetragonal (t') phase and Al_2O_3 coatings include rhombohedral (α) and cubic (γ) phases. The t' phase is a kind of no equilibrium phase which has lower c and c/a compared with the normal tetragonal (t) phase (where a, c denote the lattice parameters) and resulted from the high temperature cubic phase by a diffusionless transformation at

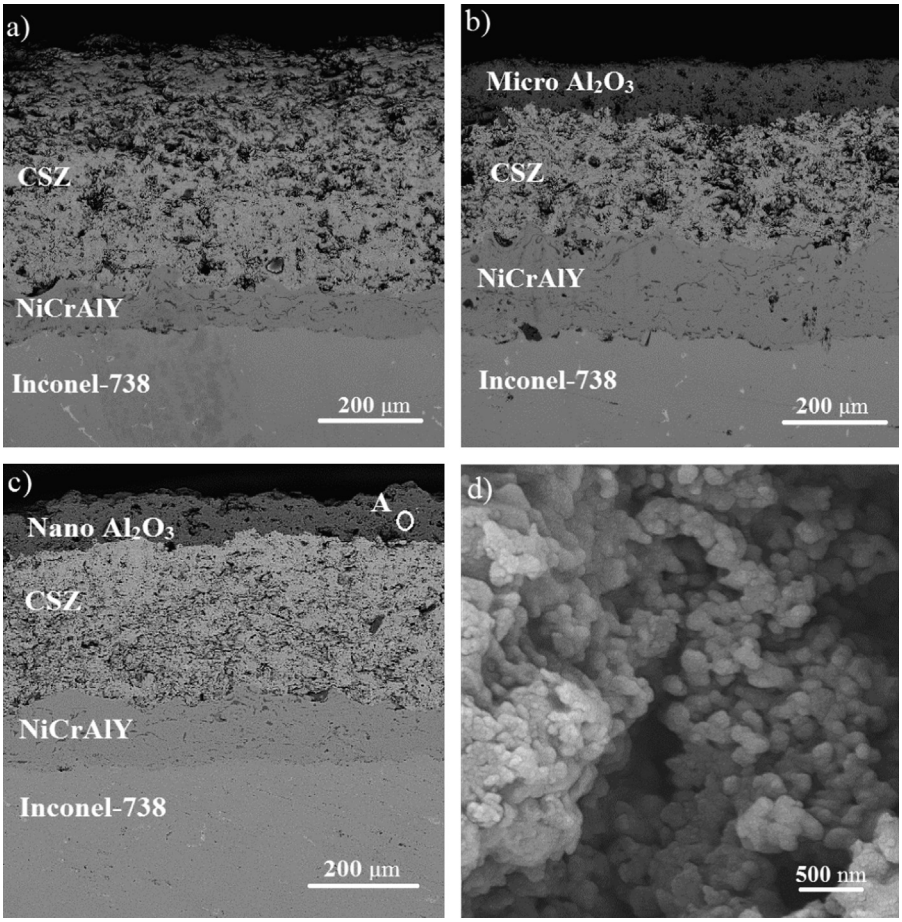

Fig. 2. SEM micrograph of polished cross section of the as-sprayed TBCs: (a) usual CSZ; (b) layer composite of CSZ/Micro Al_2O_3; (c) layer composite of CSZ/Nano Al_2O_3; (d) higher magnification of "A" region in Fig. 2(c).

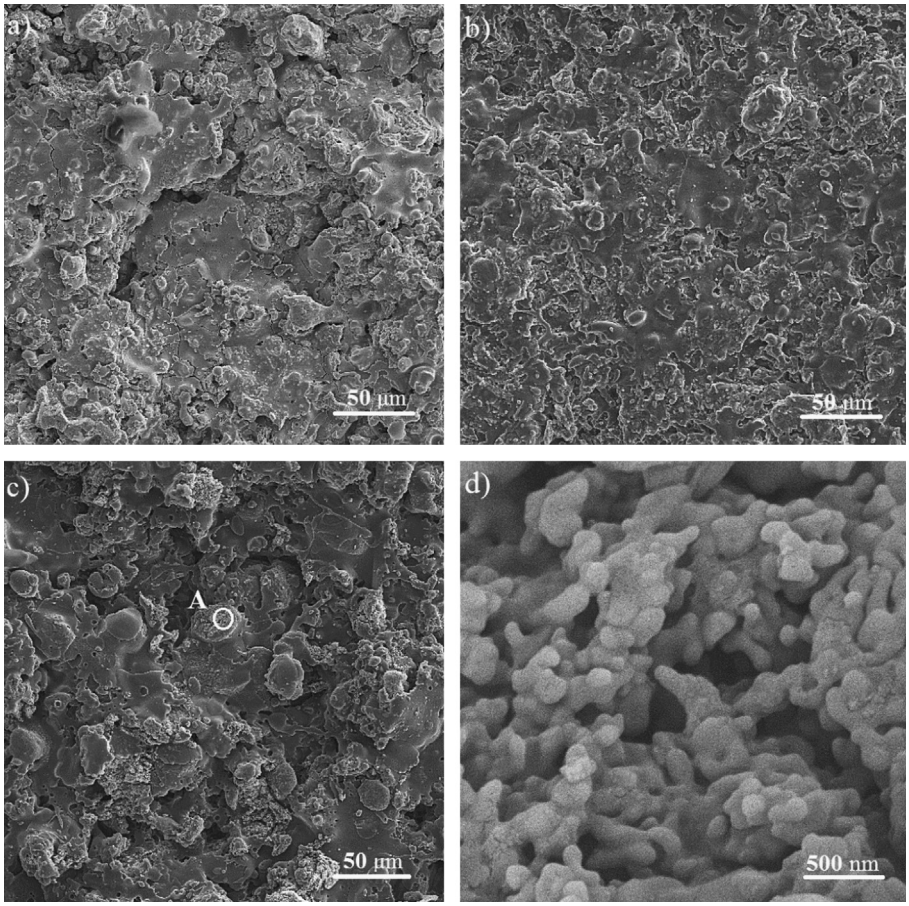

Fig. 3. SEM micrograph of top surface of the as-sprayed TBCs: (a) usual CSZ; (b) layer composite of CSZ/Micro Al_2O_3; (c) layer composite of CSZ/Nano Al_2O_3; (d) higher magnification of "A" region in Fig. 3(c).

high quenching rate of 10^6 k/s [39]. Therefore, presence of zirconia in the t' phase after plasma spraying is a common subject [39,40].

The XRD patterns of alumina layers in top surface of layer composite coatings showed that some of α-Al_2O_3 in the feedstock alumina powders was converted into γ-Al_2O_3 in effect of plasma spraying process, as presented in Fig. 4(b) and (c). It is well established that the preferential formation of γ-Al_2O_3 is attributed to the high cooling rate (about 10^6 K/s) of the molten particles during plasma spraying and easy nucleation of γ-Al_2O_3 from the melt superior to α-Al_2O_3 thanks to lower interfacial energy between crystal and liquid [41–43]. The relative amount of the major phases in alumina coatings after plasma spraying was calculated from the XRD intensity data by the following equation [42]:

$$R\,\% = \frac{I^{Y-AI_2O_8}_{(400)}}{I^{\alpha-AI_2O_8}_{(118)} + I^{Y-AI_2O_8}_{(400)}} \times 100 \quad (1)$$

where I_{hkl} is the intensity of peak diffraction for the corresponding plane of the α-Al_2O_3, and γ-Al_2O_3 phases. It was obtained that the γ-Al_2O_3 phase content (R) in the micro and nano Al_2O_3 coatings are 65.46% and 9.71%, respectively. The presence of α-Al_2O_3 in the alumina plasma sprayed coatings has been attributed to both unmelted feed particles and solid-state γ-to-α phase transformation [37]. The differences in the phase composition of micro and nano-alumina coatings after plasma spraying process according to the same plasma spray parameters for both layers can be attributed to the differences in morphology and particle size in feedstock powders before spraying. Micro Al_2O_3 powder with dense and irregularly shaped morphology has a particle size of 15–45 μm while reconstituted nano Al_2O_3 with spherical morphology has a granule size of 65–80 μm. Micro Al_2O_3 powder due to smaller and denser particles has lower heat capacity than coarser and porous granules of nano Al_2O_3 powder. The smaller granules will be melted faster that the big one, also the smaller granules can be easily accelerated and heated by the surrounding gas in the hot core of plasma. Meanwhile the larger particles tend to penetrate the core and travel around the periphery of plasma jet [42,43]. Thus the larger particles need more time to melting at same plasma spray parameters compared to smaller one. So, when exposed to the same parameters during plasma spray, it is expected that an entire micro Al_2O_3 powder particle can reach the melting point while an granule of nano Al_2O_3 powder may only partially melted or in other words it can be said that the degree of particles melting in micro Al_2O_3 layer is more than nano Al_2O_3 layer that justifies difference in the amount of gamma phase of as-sprayed micro and nano Al_2O_3 coatings.

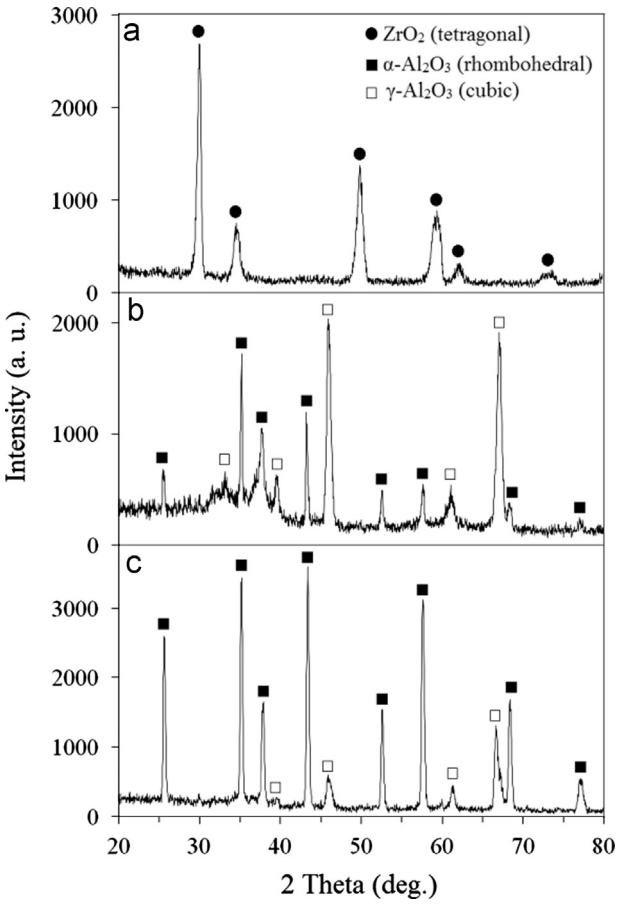

Fig. 4. XRD patterns of the as-sprayed TBCs: (a) usual CSZ; (b) layer composite of CSZ/Micro Al_2O_3; (c) layer composite of CSZ/Nano Al_2O_3.

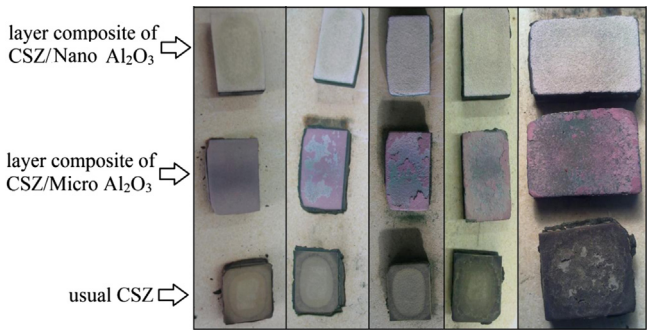

Fig. 5. Macroscopic images of coatings during hot corrosion test after: (a) 8 h; (b) 16 h; (c) 24 h; (d) 32 h; (e) 40 h.

Studies on nanostructured air plasma sprayed coatings have shown that it is paramount to carefully control the spray parameters in order to avoid the complete melting of the nanostructured granules in the plasma jet, thus preserving and embedding part of the nanostructure of granules into the coating microstructure. By controlling the amount of previously molten and porous semi-molten particles embedded in the coating microstructure, it was possible to change considerably the mechanical response of the coating. Therefore, this bimodal microstructure (caused by the coexistence of fully molten and semi-molten nanostructured granules) affected the behavior of the coating [32]. If all powder particles are fully molten in the plasma spray jet, all the nanostructural character of the powder particles will disappear, and therefore the plasma spray coating will not exhibit any nanostructural characteristics related to that of the original feedstock [44]. Finally it can be said that to achieve nanostructured coatings from nano powders required granulation for the production of porous and micron-sized granules.

3.3. Characterization of coatings after hot corrosion

Fig. 5 shows the macroscopic images of coatings during hot corrosion test. Micro alumina layer on top surface of CSZ/Micro Al_2O_3 coating and CSZ layer on top surface of usual CSZ coating spalled after 16 h and 40 h exposed to hot corrosion, respectively while no damage was found in CSZ/Nano Al_2O_3 coating.

Fig. 6 shows the SEM micrographs of top surface of coatings after 40 h hot corrosion. All three coatings revealed a porous surface. Besides CSZ/Nano Al_2O_3 coating, many crystals deposited on the surface of coatings that the shapes of these crystals are irregular shape and semi-cubic (Fig. 6(b) and (d)). In the CSZ/Micro Al_2O_3 coating, these detrimental crystals in terms of size and quantity are smaller and fewer than usual CSZ coating.

Fig. 7 illustrates the XRD patterns of coatings after 40 h hot corrosion. In usual CSZ coating, (Fig. 7(a)), zirconia is present only in the phase of monoclinic. It means that all of tetragonal zirconia phase in as-sprayed CSZ coating transformed to monoclinic phase. In CSZ/Micro Al_2O_3 coating (Fig. 7(b)) zirconia is present in tetragonal and monoclinic phases. XRD patterns of layer composite coatings after hot corrosion test (Fig. 7(b) and (c)) showed that alumina overlays did not any reaction with corrosive salts and alumina is only present in rhombohedral (α) phase. As mentioned earlier, as-sprayed Al_2O_3 overlays showed the γ and α-phases structure, and the γ-Al_2O_3 phase transformed to α-Al_2O_3 phase after exposure to hot corrosion. According to Fig. 7(a) and (b), formation of YVO_4, $CeVO_4$ and CeO_2 crystals on the surface of usual CSZ and CSZ/Micro Al_2O_3 coatings, during the hot corrosion test, is illustrated.

Fig. 8 shows the EDS analysis of B, C, D, E, F and G points of Fig. 6, that indicated porous areas with fine particles "B" contains Zr, Ce, Y and O, the irregular shape crystals "C" contain Y, Ce, V and O, the semi-cubic crystals "D" contain Ce and O, "E", "F" and "G" areas contain Al and O elements. Thus, according to SEM micrographs, EDS and XRD patterns, it is demonstrated that the porous areas with fine particles "B" is CSZ, irregular shape crystals "C" were mixture of YVO_4 and $CeVO_4$, semi-cubic crystals "D" were CeO_2, "E", "F" and "G" areas were Al_2O_3.

Monoclinic ZrO_2 and YVO_4 crystals are as hot corrosion products in YSZ coatings that caused the degradation of coating [24] while monoclinic ZrO_2, YVO_4, $CeVO_4$ and CeO_2 crystals are as hot corrosion products in CSZ (ZrO_2–25%CeO_2–2.5%Y_2O_3) coatings [15,40]. As hot corrosion

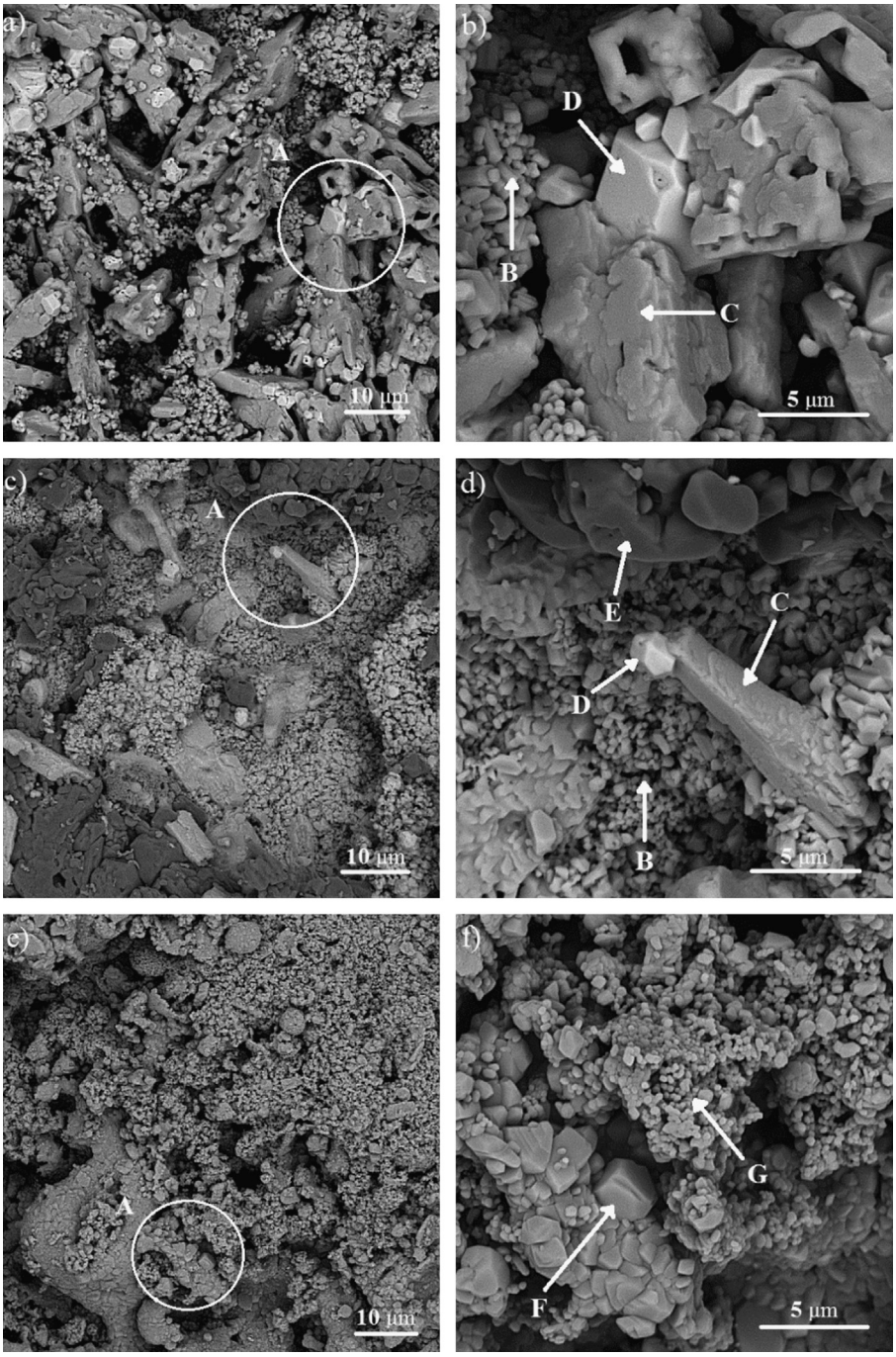

Fig. 6. SEM micrograph of top surface of TBCs after 40 h exposure to hot corrosion: (a) usual CSZ; (b) magnification of "A" region in Fig. 6(a); (c) layer composite of CSZ/Micro Al_2O_3; (d) magnification of "A" region in Fig. 6(c); (e) layer composite of CSZ/Nano Al_2O_3; (f) magnification of "A" region in Fig. 6(e).

products cause the degradation of coatings it can be concluded that hot corrosion products growth rate somehow can be indicate the rate of progress in hot corrosion process, hence, comparison the amount of hot corrosion products as the criteria for coatings destabilization during hot corrosion test in the following will be discussed.

The lack of hot corrosion products on the surface of CSZ/Nano Al_2O_3 coating after 40 h hot corrosion, indicating a better resistance to hot corrosion of this coating compared to CSZ/Micro Al_2O_3 and usual CSZ coatings.

Monoclinic ZrO_2 and irregular shape crystals of $CeVO_4$, YVO_4 were formed on usual CSZ and CSZ/Micro Al_2O_3 coatings after exposing to molten salts for 40 h at 1050 °C, but the intensity of their peaks was different.

The volume fractions of monoclinic ZrO_2 (M%) in TBCs, after hot corrosion test was estimated by the following equation [24,26,40]:

$$M\,\% = \frac{M_2 + M_2}{M_2 + M_2 + T} \times 100 \tag{2}$$

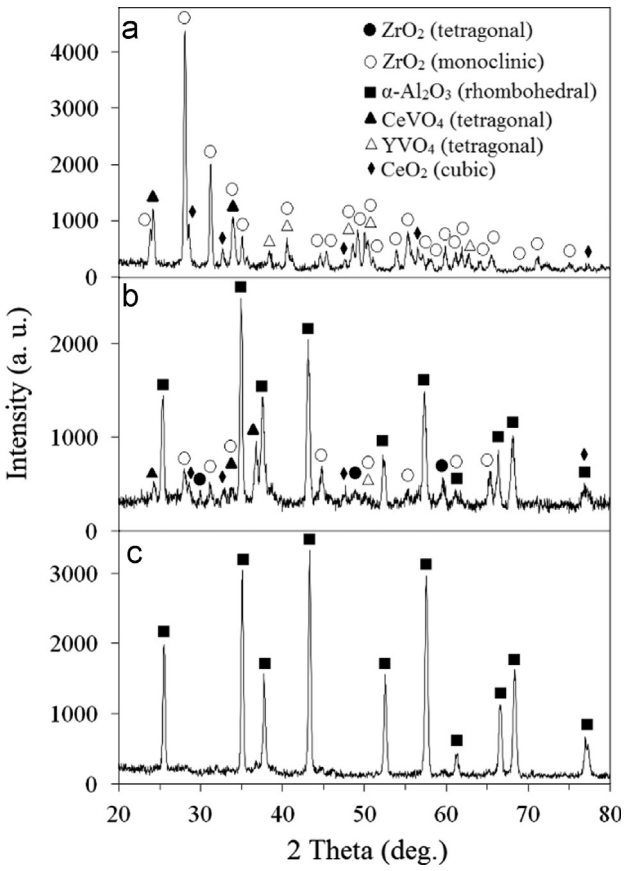

Fig. 7. XRD patterns of top surface of TBCs after 40 h exposure to hot corrosion: (a) usual CSZ; (b) layer composite of CSZ/Micro Al_2O_3; (c) layer composite of CSZ/Nano Al_2O_3.

where M_1 and M_2 are the intensity of monoclinic ZrO_2 (111) and ($\bar{1}11$) peaks, respectively, and T is the intensity of tetragonal ZrO_2 (101) peak in XRD patterns after hot corrosion test. The quantities of destabilized zirconia phase (M%) have been compared in Fig. 9. This figure shows that the volume fraction of M%-ZrO_2 decreased from 100% in usual CSZ to 75% in CSZ as inner layer of CSZ/Micro Al_2O_3 coating. This result indicates that transformation of zirconia from tetragonal to monoclinic phase in usual CSZ coating during cooling was much higher than CSZ/Micro Al_2O_3 coating.

The comparison of XRD patterns after hot corrosion (Fig. 7 (a) and (b)) shows the intensity of the main peak of $CeVO_4$ and YVO_4 in usual CSZ are significantly higher than CSZ/Micro Al_2O_3. Also this phenomenon can be corroborated by measuring the length of the irregular shape crystals according to Fig. 6 (a) and (c). Fig. 10 shows that the average length of irregular crystals of $CeVO_4$, YVO_4 in CSZ as inner layer of CSZ/Micro Al_2O_3 coating are considerably less than usual CSZ coating.

As mentioned earlier, spallation of micro Al_2O_3 layer on top surface of CSZ/Micro Al_2O_3 coating during hot corrosion occurred. Formation of hot corrosion products at the CSZ-micro Al_2O_3 interface and transformation of γ to α-Al_2O_3 caused stress and spallation of micro Al_2O_3 layer however, considering that in the nano Al_2O_3 layer with higher porosity and lower γ phase, no spallation has occurred after 40 h hot corrosion it can be said that stress arise from transformation of γ to α-Al_2O_3 is the main factor in spallation of micro Al_2O_3 layer during hot corrosion test. Thus, higher stability of nano Al_2O_3 layer compared to micro Al_2O_3 layer during hot corrosion cycles can be attributed to the lower γ phase in as-sprayed nano Al_2O_3 layer and consequently the lower stresses due to from γ → α-Al_2O_3 transformation.

3.4. Investigation of possible reactions

Comprehension of hot corrosion mechanism of CSZ coatings by corrosive salts (55 wt% V_2O_5 and 45 wt% Na_2SO_4), requires analysis of the reactions. Therefore, in the following investigation of the possible reactions are discussed:

In the beginning, $NaVO_3$ was formed after the reaction of sodium sulfate and vanadium oxide at high temperature by the following reactions [45]:

$$Na_2SO_4\ (l) \rightarrow Na_2O\ (l) + SO_3\ (g) \quad (3)$$

$$Na_2O\ (l) + V_2O_5\ (l) \rightarrow 2NaVO_3\ (l) \quad (4)$$

Then $NaVO_3$ reacted with stabilizer of ZrO_2 (Y_2O_3) to form monoclinic ZrO_2, YVO_4 and Na_2O [46]:

$$ZrO_2\ (Y_2O_3)\ (s) + 2NaVO_3\ (l) \rightarrow ZrO_2\ (\text{monoclinic})\ (s) + 2YVO_4\ (s) + Na_2O\ (l) \quad (5)$$

In EDS analysis which was performed on different points of coating surface, Na was not detected. It seems that Na_2O is sublimated due to high temperature in hot corrosion considering that this result is in agreement with previous investigations [24,40]. Also it has been reported [45,47] that V_2O_5 can react directly with Y_2O_3 to form YVO_4 and monoclinic ZrO_2 by the following reaction:

$$ZrO_2\ (Y_2O_3)\ (s) + V_2O_5\ (l) \rightarrow ZrO_2\ (\text{monoclinic})\ (s) + 2YVO_4\ (s) \quad (6)$$

Laboratory tests confirmed that CeO_2 (presumably because of its greater Lewis acidity) is more resistance to chemical reaction with $NaVO_3$ than Y_2O_3 [21] or other laboratory tests indicated that CeO_2 is not chemically reacted with molten $NaVO_3$ salt [48]. However, Park et al. [15] demonstrated that both the free CeO_2 precipitates and CeO_2 stabilizers remaining in zirconia reacted with the $NaVO_3$ salt to form $CeVO_4$.

Other laboratory tests reported that the destabilization of CSZ by pure molten $NaVO_3$ is therefore evidently a mineralization effect. In contrast, when CSZ is destabilized by V_2O_5 or $NaVO_3$–V_2O_5 mixtures, the reaction product, $CeVO_4$, is found, which indicates destabilization in this case to be occurring by chemical reaction [45].

No evidence from XRD patterns was found to indicate that the chemical reaction between Na_2SO_4 and CSZ had taken place. Zhong et al. [27] also confirmed that Na_2SO_4 had no chemical effect on YSZ coating at the elevated temperature of 1000 °C.

Chen et al.'s investigation [49] on hot corrosion of plasma sprayed ZrO_2 coating with Al_2O_3 overlay in molten salt

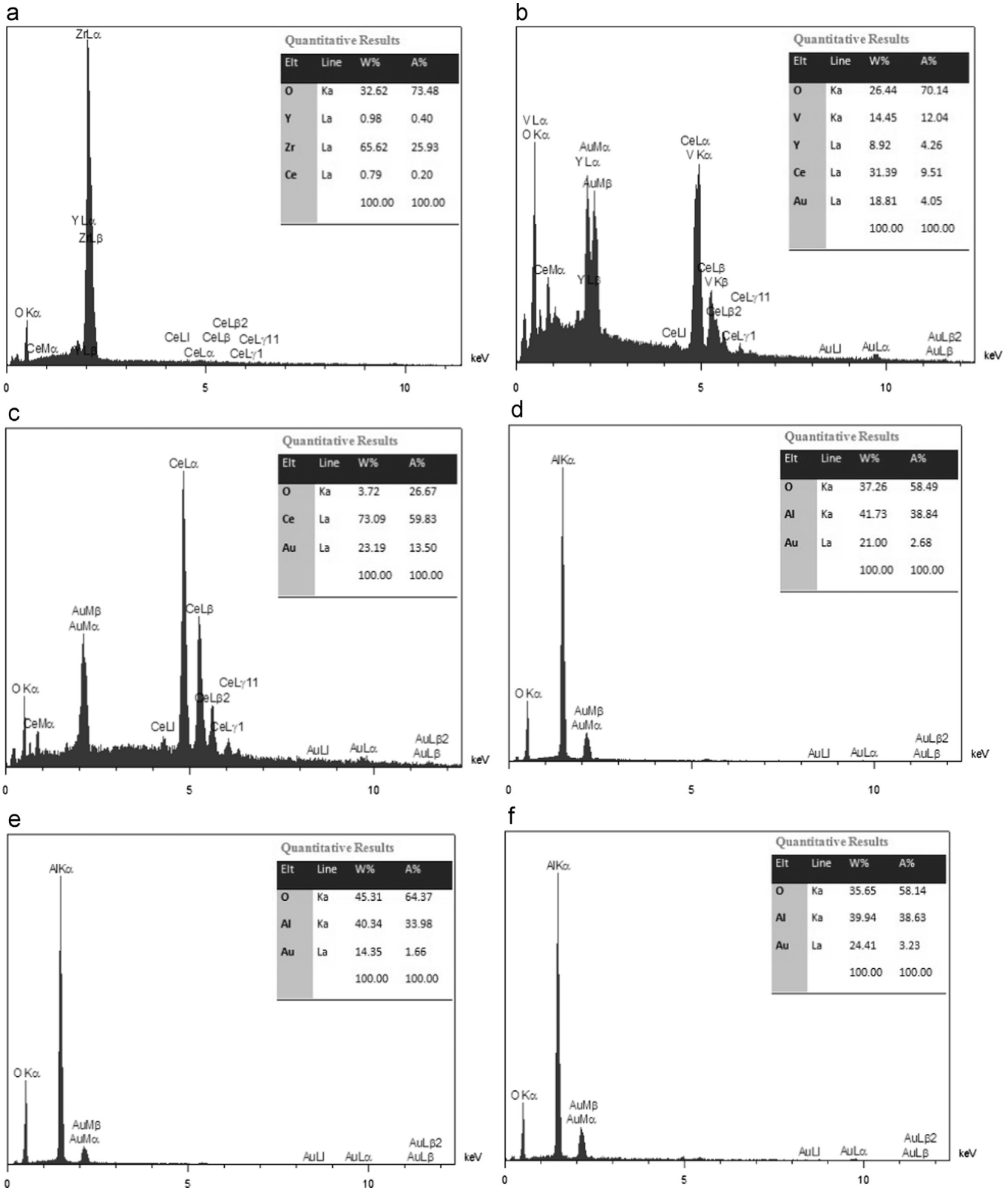

Fig. 8. EDS analysis of (a) B; (b) C; (c) D; (d) E; (e) F; (f) G points as shown in Fig. 6.

mixtures ($Na_2O_4+5\%V_2O_5$) showed that $NaAlO_2$ can be formed on the surface of Al_2O_3 particles as a protective against hot corrosion by the following reactions:

$$Na_2SO_4\ (l) \rightarrow Na_2O\ (l) + SO_3\ (g) \quad (7)$$

$$Al_2O_3\ (s) + Na_2O\ (l) \rightarrow 2NaAlO_2\ (s) \quad (8)$$

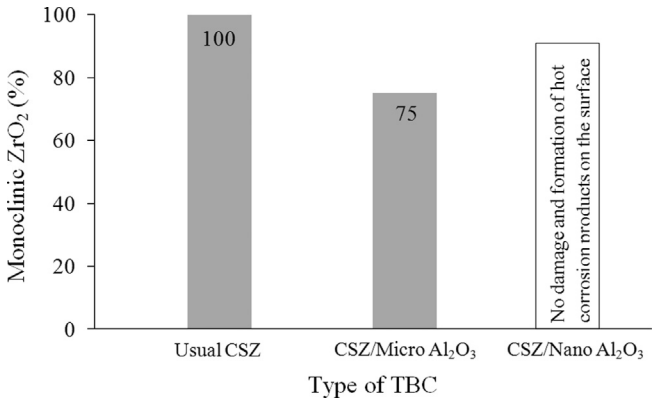

Fig. 9. Volume fraction of monoclinic zirconia in the coatings after hot corrosion.

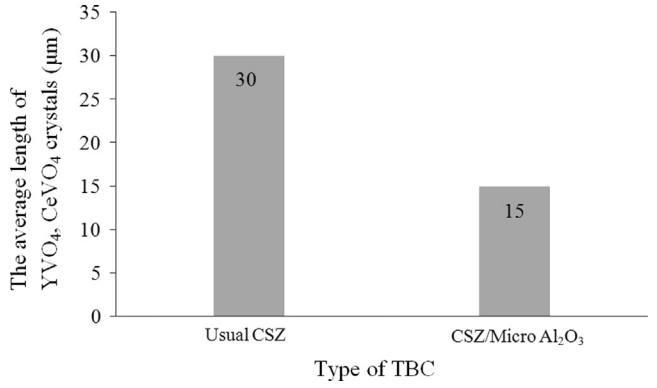

Fig. 10. The average length of irregular shape crystals of YVO_4, $CeVO_4$ in TBCs after 40 h hot corrosion test at 1050 °C.

In the present study, $NaAlO_2$ was not detected by XRD analysis, thus it cannot be said that Al_2O_3 overlays are protected by $NaAlO_2$ compound during hot corrosion.

3.5. Hot corrosion mechanism of CSZ coatings

The hot corrosion behavior and failure mechanism of CSZ coating in the present study involve the following steps that are in agreement with previous investigations [45,50]:

(1) Infiltration of molten salts through coating's defects (micro cracks, open pores and inter splat voids).
(2) Interaction of molten salts with stabilizers of zirconia (Y_2O_3 and CeO_2):
   (I) Chemical reaction of V_2O_5 or $NaVO_3$–V_2O_5 mixtures with stabilizers to formation of YVO_4, $CeVO_4$ irregular shape crystals.
   (II) Mineralization of CeO_2 by pure $NaVO_3$ to formation of semi-cubic crystals.
   Phase transformation of t-ZrO_2 to m-ZrO_2 due to stabilizers depletion, which is accompanied by a large destruc-
(3) tive volume expansion of the coating.
(4) Formation of monoclinic ZrO_2, semi-cubic CeO_2 crystals and irregular shape crystals of YVO_4, $CeVO_4$ with outward growth in usual CSZ coating as hot corrosion products that caused creation of additional stresses and cracks in the coating.

In addition, this investigation illustrates the following procedures during degradation of three types of TBCs by hot corrosion:

- Formation and growth of semi-cubic CeO_2 crystals, irregular shape YVO_4, $CeVO_4$ crystals up to average lengths of 5 and 30 μm respectively and formation of monoclinic ZrO_2 in usual CSZ as hot corrosion products.
- Spallation of CSZ layer on top surface of usual CSZ after 40 h hot corrosion due to stresses arise from formation of hot corrosion products.
- Delaminating of micro Al_2O_3 layer on top surface of CSZ/Micro Al_2O_3 coating after 16 h hot corrosion due to transformation of γ to α-Al_2O_3 phase.

In plasma sprayed TBCs, existence of some porosity is necessary to provide thermal insulation and thermal shock resistance [51]. These porosities provide the possibility of infiltration of corrosive salts into TBCs structure and then these corrosive salts reacts with stabilizers of partially stabilized zirconia coating and caused destabilization of zirconia coating, therefore, it can be said that porosities play an important role in hot corrosion behavior of TBCs.

In this research plasma spraying of nano and micro Al_2O_3 layer with porosity of 3.2% and 4.4% respectively, were produced on top surface of CSZ coating with 10.6% porosity. The chemically inertness and dense Al_2O_3 overlay on usual CSZ coating reduced the infiltration of molten salts into CSZ layer and considerably decreased depletion of stabilizers (Y_2O_3 and CeO_2) from this layer and consequently improved hot corrosion resistance of usual CSZ coating, although achieving this improvement was higher by nano Al_2O_3 overlay in comparison with micro Al_2O_3 overlay due to greater stability of nano than micro Al_2O_3 layer during hot corrosion test.

4. Conclusion

(1) After 40 h exposure to hot corrosion, no damage and hot corrosion products was found on the surface of CSZ/Nano Al_2O_3 coating and monoclinic ZrO_2 fraction was lower in CSZ/Micro Al_2O_3 coating in comparison with usual CSZ.
(2) In hot corrosion test, reaction of molten salts with stabilizers of zirconia (Y_2O_3 and CeO_2) that accompanied by formation of monoclinic zirconia, irregular shape crystals of YVO_4, $CeVO_4$ and semi-cubic crystals of CeO_2 as hot corrosion products, caused the degradation of CSZ coating.
(3) Nano Al_2O_3 coating showed higher stability in hot corrosion cycles than micro Al_2O_3 coating that can be attributed to the lower γ phase in as-sprayed nano Al_2O_3 coating.
(4) In the layer composite coatings, the presence of a dense Al_2O_3 overlay on CSZ reduced the infiltration of molten

salts into CSZ coating and had a significant effect on increasing of hot corrosion resistance of TBCs.

References

[1] V. Teixeira, M. Andritschky, W. Fischer, H. Buchkremer, D. Stöver, Effects of deposition temperature and thermal cycling on residual stress state in zirconia-based thermal barrier coatings, Surface and Coatings Technology 120 (1999) 103–111.

[2] A. Portinha, V. Teixeira, J. Carneiro, J. Martins, M. Costa, R. Vassen, D. Stoever, Characterization of thermal barrier coatings with a gradient in porosity, Surface and Coatings Technology 195 (2005) 245–251.

[3] S. Das, S. Datta, D. Basu, G. Das, Glass–ceramics as oxidation resistant bond coat in thermal barrier coating system, Ceramics International 35 (2009) 1403–1406.

[4] Y. Li, Y. Xie, X. Liu, X. Zheng, Effect of physical vapor deposited Al_2O_3 film on TGO growth in YSZ/CoNiCrAlY coatings, Ceramics International 38 (2012) 5113–5121.

[5] R. Vaßen, M.O. Jarligo, T. Steinke, D.E. Mack, D. Stöver, Overview on advanced thermal barrier coatings, Surface and Coatings Technology 205 (2010) 938–942.

[6] M. Alfano, G. Di Girolamo, L. Pagnotta, D. Sun, Processing, microstructure and mechanical properties of air plasma-sprayed ceria–yttria co-stabilized zirconia coatings, Strain 46 (2010) 409–418.

[7] J. Fenech, C. Viazzi, J.-P. Bonino, F. Ansart, A. Barnabé, Morphology and structure of YSZ powders: comparison between xerogel and aerogel, Ceramics International 35 (2009) 3427–3433.

[8] S. Guo, Y. Kagawa, Effect of thermal exposure on hardness and Young's modulus of EB-PVD yttria-partially-stabilized zirconia thermal barrier coatings, Ceramics international 32 (2006) 263–270.

[9] R. Steinbrech, V. Postolenko, J. Mönch, J. Malzbender, L. Singheiser, Testing method to assess lifetime of EB-PVD thermal barrier coatings on tubular specimens in static and cyclic oxidation tests, Ceramics International 37 (2011) 363–368.

[10] X. Chen, Y. Zhao, X. Fan, Y. Liu, B. Zou, Y. Wang, H. Ma, X. Cao, Thermal cycling failure of new $LaMgAl_{11}O_{19}$/YSZ double ceramic top coat thermal barrier coating systems, Surface and Coatings Technology 205 (2011) 3293–3300.

[11] Y. Bai, Z. Han, H. Li, C. Xu, Y. Xu, Z. Wang, C. Ding, J. Yang, High performance nanostructured ZrO_2 based thermal barrier coatings deposited by high efficiency supersonic plasma spraying, Applied Surface Science 257 (2011) 7210–7216.

[12] S. Raghavan, M.J. Mayo, The hot corrosion resistance of 20 mol% $YTaO_4$ stabilized tetragonal zirconia and 14 mol% Ta_2O_5 stabilized orthorhombic zirconia for thermal barrier coating applications, Surface and Coatings Technology 160 (2002) 187–196.

[13] B. Nagaraj, D. Wortman, Burner rig evaluation of ceramic coatings with vanadium-contaminated fuels, Journal of Engineering for Gas Turbines and Power 112 (1990) 536–542.

[14] R.L. Jones, D. Mess, India as a hot corrosion-resistant stabilizer for zirconia, Journal of the American Ceramic Society 75 (1992) 1818–1821.

[15] S. Park, J. Kim, M. Kim, H. Song, C. Park, Microscopic observation of degradation behavior in yttria and ceria stabilized zirconia thermal barrier coatings under hot corrosion, Surface and Coatings Technology 190 (2005) 357–365.

[16] C.H. Lee, H.K. Kim, H.S. Choi, H.S. Ahn, Phase transformation and bond coat oxidation behavior of plasma-sprayed zirconia thermal barrier coating, Surface and Coatings Technology 124 (2000) 1–12.

[17] H. Choi, H. Kim, C. Lee, Phase evolutions of plasma sprayed ceria and yttria stabilized zirconia thermal barrier coating, Journal of Materials Science Letters 21 (2002) 1359–1361.

[18] P. Huang, J. Swab, P. Patel, W. Chu, Evaluation of CeSZ thermal barrier coatings for diesels, in: Proceedings of the ITSC 2000: 1st International Thermal Spray Conference, 2000, pp. 1179–1183.

[19] P. Mohan, B. Yuan, T. Patterson, V.H. Desai, Y.H. Sohn, Degradation of yttria-stabilized zirconia thermal barrier coatings by vanadium pentoxide, phosphorous pentoxide, and sodium sulfate, Journal of the American Ceramic Society 90 (2007) 3601–3607.

[20] P. Mohan, T. Patterson, B. Yao, Y. Sohn, Degradation of thermal barrier coatings by fuel impurities and CMAS: thermochemical interactions and mitigation approaches, Journal of Thermal Spray Technology 19 (2010) 156–167.

[21] R. Jones, C. Williams, A. Jones, Reaction of vanadium compounds with ceramic oxides, Journal of The Electrochemical Society; (United States) 133 (1986) 227–230.

[22] R. Jones, Oxide acid-base reactions relating to the inhibition of vanadium attack on REY zeolite catalysts, Journal of Catalysis 129 (1991) 269–274.

[23] R. Stevens, An Introduction to Zirconia, Magnesium Elektron Limited, London, 1983.

[24] A. Afrasiabi, M. Saremi, A. Kobayashi, A comparative study on hot corrosion resistance of three types of thermal barrier coatings: YSZ, YSZ+Al_2O_3 and YSZ/Al_2O_3, Materials Science and Engineering: A 478 (2008) 264–269.

[25] Z. Chen, N. Wu, J. Singh, S. Mao, Effect of Al_2O_3 overlay on hot-corrosion behavior of yttria-stabilized zirconia coating in molten sulfate–vanadate salt, Thin solid films 443 (2003) 46–52.

[26] X. Chen, Y. Zhao, L. Gu, B. Zou, Y. Wang, X. Cao, Hot corrosion behaviour of plasma sprayed YSZ/$LaMgAl_{11}O_{19}$ composite coatings in molten sulfate–vanadate salt, Corrosion Science 53 (2011) 2335–2343.

[27] X. Zhong, Y. Wang, Z. Xu, Y. Zhang, J. Zhang, X. Cao, Hot-corrosion behaviors of overlay-clad yttria-stabilized zirconia coatings in contact with vanadate–sulfate salts, Journal of the European Ceramic Society 30 (2010) 1401–1408.

[28] A. Afrasiabi, A. Kobayashi, Hot corrosion control in plasma sprayed YSZ coating by alumina layer with evaluation of microstrcuture and nanoindentation data (H, E), Vacuum 88 (2013) 103–107.

[29] S.X. Mao, Impermeable Thin Al_2O_3 Overlay for TBC Protection From Sulfate and Vanadate Attack in Gas Turbines, National Energy Technology Lab., Pittsburgh, PA (US), National Energy Technology Lab, Morgantown, WV (USA), 2002.

[30] A. Afrasiabi, A. Kobayashi, The effect of an additional alumina layer in improvement of plasma sprayed TBCs during high temperature applications, Transactions of JWRI 37 (2008) 57–61.

[31] S. Aruna, N. Balaji, J. Shedthi, V. Grips, Effect of critical plasma spray parameters on the microstructure, microhardness and wear and corrosion resistance of plasma sprayed alumina coatings, Surface and Coatings Technology 208 (2012) 92–100.

[32] H. Xu, H. Guo, in: Thermal Barrier Coatings, Woodhead Publishing, Philadelphia, USA, 2011.

[33] H. Chen, C. Ding, Nanostructured zirconia coating prepared by atmospheric plasma spraying, Surface and Coatings Technology 150 (2002) 31–36.

[34] H. Chen, C. Ding, P. Zhang, P. La, S.W. Lee, Wear of plasma-sprayed nanostructured zirconia coatings against stainless steel under distilled-water conditions, Surface and Coatings Technology 173 (2003) 144–149.

[35] E.H. Jordan, M. Gell, Y. Sohn, D. Goberman, L. Shaw, S. Jiang, M. Wang, T. Xiao, Y. Wang, P. Strutt, Fabrication and evaluation of plasma sprayed nanostructured alumina–titania coatings with superior properties, Materials Science and Engineering: A 301 (2001) 80–89.

[36] H. Jamali, R. Mozafarinia, R. Shoja Razavi, R. Ahmadi-Pidani, M. Reza Loghman-Estarki, Fabrication and evaluation of plasma-sprayed nanostructured and conventional YSZ thermal barrier coatings, Current Nanoscience 8 (2012) 402–409.

[37] D. Goberman, Y. Sohn, L. Shaw, E. Jordan, M. Gell, Microstructure development of Al_2O_3–13 wt% TiO_2 plasma sprayed coatings derived from nanocrystalline powders, Acta Materialia 50 (2002) 1141–1152.

[38] V. Chawla, B.S. Sidhu, D. Puri, S. Prakash, State of art: plasma sprayed nanostructured coatings: a review, Materials Forum 38 (2008) 137–143.

[39] L. Wang, Y. Wang, X. Sun, J. He, Z. Pan, C. Wang, Thermal shock behavior of 8YSZ and double-ceramic-layer $La_2Zr_2O_7$/8YSZ thermal barrier coatings fabricated by atmospheric plasma spraying, Ceramics International 38 (2012) 3595–3606.

[40] R. Ahmadi-Pidani, R. Shoja-Razavi, R. Mozafarinia, H. Jamali, Evaluation of hot corrosion behavior of plasma sprayed ceria and yttria stabilized zirconia thermal barrier coatings in the presence of $Na_2SO_4+V_2O_5$ molten salt, Ceramics International 38 (2012) 6613–6620.

[41] Y. Zeng, S. Lee, C. Ding, Plasma spray coatings in different nanosize alumina, Materials Letters 57 (2002) 495–501.

[42] L. Marcinauskas, Deposition of alumina coatings from nanopowders by plasma spraying, Materials Science 16 (2010) 47–51.

[43] Z. Yin, S. Tao, X. Zhou, C. Ding, Particle in-flight behavior and its influence on the microstructure and mechanical properties of plasma-sprayed Al_2O_3 coatings, Journal of the European Ceramic Society 28 (2008) 1143–1148.

[44] R.S. Lima, B.R. Marple, Thermal spray coatings engineered from nanostructured ceramic agglomerated powders for structural, thermal barrier and biomedical applications: a review, Journal of Thermal Spray Technology 16 (2007) 40–63.

[45] R.L. Jones, Some aspects of the hot corrosion of thermal barrier coatings, Journal of Thermal Spray Technology 6 (1997) 77–84.

[46] C. Batista, A. Portinha, R. Ribeiro, V. Teixeira, C. Oliveira, Evaluation of laser-glazed plasma-sprayed thermal barrier coatings under high temperature exposure to molten salts, Surface and Coatings Technology 200 (2006) 6783–6791.

[47] I. Gurrappa, Thermal barrier coatings for hot corrosion resistance of CM 247 LC superalloy, Journal of Materials Science Letters 17 (1998) 1267–1269.

[48] Z. Xu, L. He, R. Mu, S. He, G. Huang, X. Cao, Hot corrosion behavior of rare earth zirconates and yttria partially stabilized zirconia thermal barrier coatings, Surface and Coatings Technology 204 (2010) 3652–3661.

[49] H. Chen, Z. Liu, Y. Chuang, Degradation of plasma-sprayed alumina and zirconia coatings on stainless steel during thermal cycling and hot corrosion, Thin solid films 223 (1993) 56–64.

[50] R.L. Jones, Experiences in Seeking Stabilizers for Zirconia Having Hot Corrosion-Resistance and High Temperature Tetragonal (t') Stability, DTIC Document, 1996.

[51] S.G. Terry, J.R. Litty, C.G. Levi, evolution of porosity and texture in thermal barrier coatings grown by eb-pvd, elevated temperature coatings, science and technology III, in: Proceedings of TMS Annual Meeting, The Minerals, Metals and Materials Society, Warrendale, USA, 1999, pp. 13–25.